



Contents lists available at ScienceDirect

Journal of Quantitative Spectroscopy & Radiative Transfer

journal homepage: www.elsevier.com/locate/jqsrt

Modelling of different TIRM setups by the Discrete Sources Method

Natalia Grishina^{a,*}, Elena Eremina^b, Yuri Eremin^a, Thomas Wriedt^c^a Moscow Lomonosov State University, Vorobyov's Hills, 119991 Moscow, Russia^b University of Bremen, Badgasteiner str. 3, 28359 Bremen, Germany^c Institute of Materials' science, Badgasteiner str. 3, 28359 Bremen, Germany

ARTICLE INFO

Available online 12 January 2011

Keywords:

Total internal reflection microscopy (TIRM)

Filmed surface

Discrete sources method

Evanescent wave scattering

Layered interface

ABSTRACT

Total Internal Reflection Microscopy (TIRM) is an effective technique to measure weak interaction forces between colloidal particles in solution and a flat surface. In this paper the Discrete Sources Method has been applied to model different measuring schemes for TIRM to find the most appropriate one for the determination of the distance between a particle and the filmed surface. It has been found that the placing of a light collector beneath the prism gives a considerable advantage compared with a conventional TIRM design, where the collector is situated above the surface.

© 2011 Elsevier Ltd. All rights reserved.

1. Introduction

Total Internal Reflection Microscopy (TIRM) appeared in the eighties as an effective technique for measuring particle-wall interaction forces. Due to the use of the Brownian fluctuations of a free colloidal particle for obtaining the interaction potential, TIRM allows to measure forces with a resolution up to 1 nm [1,2], which is advantageous compared to other techniques similar to Atomic Force Microscopy [3]. In contrast to Photonic Force Microscopy (PFM) [4,5], which is able to measure femtonewton forces as well, TIRM allows measurements close to a surface [6–8], while the PFM is applicable just to bulk measurements far from surfaces. Recently TIRM has been extended for measurements of van der Waals [9], Casimir [10], magnetic [11], depletion [12,13] and electrostatic [14] forces.

In the beginning of TIRM measurements the reconstruction of the interaction potential was based on the simple assumption that the intensity of the field scattered by a particle is proportional to the intensity of an evanescent exciting field in the particle domain. Later

measurements showed disagreement with the behavior predicted by this simple model [15]. Recently, the simple assumption has been corrected by using a rigorous scattering model, based on the Discrete Sources Method (DSM) [16]. It has been proved that employing the DSM model allows reconstruction of the potential with high precision [15,17,18]. In a particular case the reconstruction of the interaction potential has been done by comparing the measured results with the simulated results computed by the DSM model.

In conventional TIRM setups the colloidal particle is situated above the glass prism. The laser beam propagating from the prism to the surface with an angle slightly above the angle of total internal reflection generates an evanescent field in the area above the prism. In the TIRM schemes the scattered light is collected by the objective placed above the particle in the far zone (Fig. 1A). Recently it has been suggested to place the light collector in the area beneath the glass prism. In this case the collecting objective is oriented toward the beam, which is reflected from the prism surface (Fig. 1B). To reduce the intensity of the reflected beam the effect of Plasmon Resonance (PR) in a thin gold film, deposited on the prism surface, can be employed [19].

In the present paper the DSM has been applied to model suggested TIRM schemes and to compare their

* Corresponding author. Tel.: +7 495 336 0346; fax: +7 495 939 1776.
E-mail address: ngrishina@inbox.ru (N. Grishina).

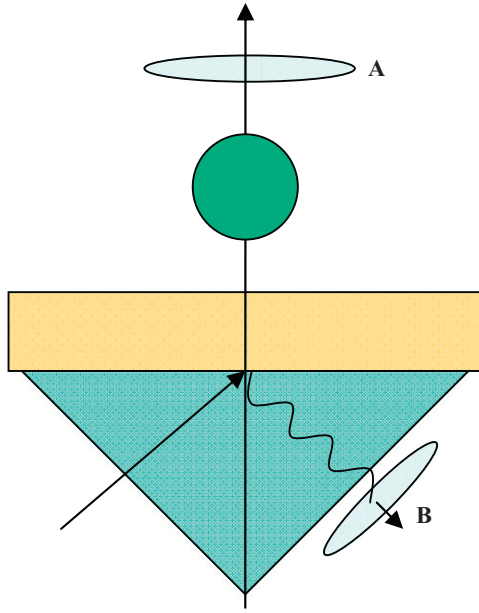


Fig. 1. Model geometry: objective disposition for the case of conventional setup (A); alternative setup (B).

efficiency. The direct comparison allows choosing the scheme that is more appropriate for the determination of the particle–film distance.

2. Discrete sources method outlines

In this section the DSM model for the evanescent wave scattering analysis is considered. We start with the mathematical statement of the polarized light scattering problem. Consider an axial symmetric penetrable particle with an interior domain D_i and a smooth boundary ∂D_i that is deposited above the plane surface Σ_1 ($z=d$) (Fig. 2).

We denote the prism domain by D_0 and an ambient space exterior to the particle by D_2 . Let us introduce a Cartesian coordinate system $Oxyz$ by choosing its origin O at the intersection point of the axis of symmetry of the particle and the plane Σ_0 ($z=0$). The Z -axis coincides with the axis of symmetry of the particle and is directed into the domain D_2 . A noble metal film occupying domain D_1 with upper boundary Σ_1 ($z=d$) is located on a planar surface Σ_0 of a glass prism. We assume that the exciting field $\{\mathbf{E}^0, \mathbf{H}^0\}$ is a linear polarized plane wave propagating inside the glass prism at angle θ_0 with respect to the z -axis. According to Snell's law the wave $\{\mathbf{E}_2^i, \mathbf{H}_2^i\}$ refracted into D_2 propagates at angle θ_2 to the Z -axis. Then the mathematical statement of the scattering problem can be formulated in the following form:

$$\begin{aligned} \nabla \times \mathbf{H}_l &= jk\epsilon_l \mathbf{E}_l, \quad \nabla \times \mathbf{E}_l = -jk\mu_l \mathbf{H}_l, \quad \text{in } D_l, \quad l=0,1,2,i \\ \mathbf{n}_i \times (\mathbf{E}_i - \mathbf{E}_2) &= 0 \quad \mathbf{n}_i \times (\mathbf{H}_i - \mathbf{H}_2) = 0 \quad \text{at } \partial D_i \\ \mathbf{e}_z \times (\mathbf{E}_{l+1} - \mathbf{E}_l) &= 0 \quad \mathbf{e}_z \times (\mathbf{H}_{l+1} - \mathbf{H}_l) = 0 \quad \text{at } \Sigma_l \text{ where } l=0,1 \end{aligned} \quad (1)$$

plus radiation conditions at infinity in D_2 and attenuation conditions in D_1 .

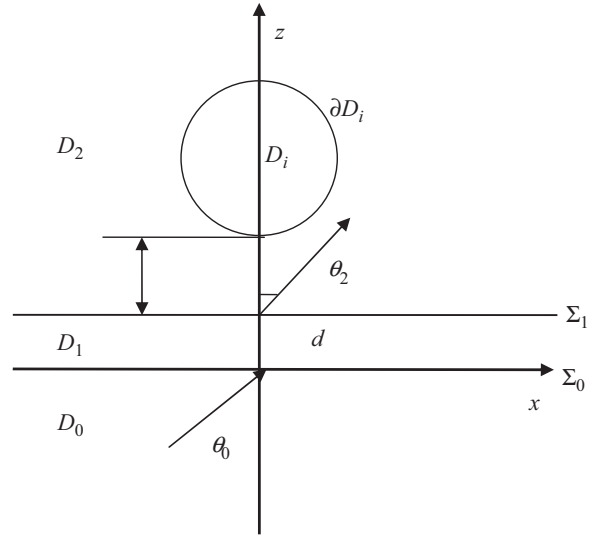


Fig. 2. Model geometry: particle deposited on a filmed prism surface.

Here, \mathbf{n}_i is the outward unit normal vector to ∂D_i , $k=\omega/c$ and $\{\mathbf{E}_l, \mathbf{H}_l\}$ stand for the total field in the corresponding domain D_l , \mathbf{e}_z is the unit vector along Z -axis. Note that the total field in D_2 is a superposition of the refracted exciting field and the scattered one, that $\mathbf{E}_2 = \mathbf{E}_2^s + \mathbf{E}_2^i$, $\mathbf{H}_2 = \mathbf{H}_2^s + \mathbf{H}_2^i$. If $\text{Im}\epsilon_l, \mu_l \leq 0$ (time dependence for the fields is chosen as $\exp[j\omega t]$) and the particle surface is smooth enough, $\partial D_i \in C^{(2,\infty)}$, then the above boundary-value problem is uniquely solvable.

The solution of the boundary value problem is constructed following the DSM scheme [16]. First the transmission problem of the plane wave on the layered interface is solved. The resulting field $\{\mathbf{E}_l^i, \mathbf{H}_l^i\}$ satisfies the transmission conditions at $\Sigma_{0,1}$. Then we construct an approximate solution to the scattering problem (1) via the DSM by representing the electromagnetic fields as a finite linear combination of the fields of dipoles and multipoles, which satisfy analytically the transmission conditions enforced at the plane interfaces $\Sigma_{0,1}$ [16]. The approximate solution satisfies the Maxwell equations in the domains D_l , $l=0,1,2$, infinity conditions and the transmission conditions at the interfaces $\Sigma_{0,1}$. Thus, the scattering problem is reduced to the problem of approximating the exciting field at the particle surface ∂D_i . The amplitudes of the discrete sources (DS) are determined from the boundary conditions at the particle surface, which can be rewritten as

$$\mathbf{n}_i \times (\mathbf{E}_i - \mathbf{E}_2^s) = \mathbf{n}_i \times \mathbf{E}_2^i, \quad \mathbf{n}_i \times (\mathbf{H}_i - \mathbf{H}_2^s) = \mathbf{n}_i \times \mathbf{H}_2^i \quad \text{at } \partial D_i, \quad (2)$$

To construct the fields of dipoles and multipoles that analytically satisfy the transmission conditions at the plane interfaces $\Sigma_{0,1}$ we incorporate the Green's tensor for a stratified interface [16].

The approximate solution of the scattering problem is constructed fulfilling the transmission conditions and the plane interfaces $\Sigma_{0,1}$ taking into account the rotational symmetry of the scattering problem geometry (particle

plus layered interface) and the polarization of the exciting field [20].

Now let us consider a P-polarized exciting plane wave. In this case, the refracted plane wave in D_2 accepts the following form:

$$\mathbf{E}_2^i(\mathbf{r}) = T_2^p(-\mathbf{e}_x \cos \theta_2 + \mathbf{e}_z \sin \theta_2) \exp\{-jk_2(x \sin \theta_2 + z \cos \theta_2)\},$$

$$\mathbf{H}_2^i(\mathbf{r}) = T_2^p n_2 \mathbf{e}_y \exp\{-jk_2(x \sin \theta_2 + z \cos \theta_2)\}, \quad (3)$$

where $(\mathbf{e}_x, \mathbf{e}_y, \mathbf{e}_z)$ are unit vectors of the Cartesian coordinate system, $n_2 = \sqrt{\varepsilon_2 \mu_2}$ is the refractive index of the ambient space, $k_2 = kn_2$ and T_2^p is the transmission coefficient for P-polarization associated with the multi-layered interface. Following Snell's law: $n_0 \sin \theta_0 = n_2 \sin \theta_2$. If $\theta_0 > \theta_c = \arcsin(n_2/n_0)$ the exciting wave is totally reflected from the plane Σ_1 and only an evanescent wave propagates along the surface Σ_1 and damped by the \mathbf{e}_z direction is presented in D_2 . In this particular case $\cos \theta_2$ becomes purely imaginary.

We must choose its value as $\cos \theta_2 = -j\sqrt{\sin^2 \theta_2 - 1}$, otherwise the amplitude of the refracted wave would tend to infinity with increasing distance from the interface Σ_1 . So, the plane wave amplitude takes the form $\exp\{-jk_2 x \sin \theta_2\} \exp\{-k_2 z \sqrt{\sin^2 \theta_2 - 1}\}$.

As mentioned above, the approximate solution of the scattering problem is constructed by taking into account not only the rotational symmetry of the scattering problem geometry, but the polarization of the external excitation as well [20].

For P-polarized excitation we will use the Fourier series for the plane wave with respect to the azimuth angle φ :

$$\exp\{-jk_2 \rho \sin \theta_2 \cos \varphi\} = \sum_{m=0}^{\infty} (2 - \delta_{0m}) (-j)^m J_m(k_2 \rho \sin \theta_2) \cos m \varphi$$

Here J_m is a cylindrical Bessel function of m -th order, δ_{0m} is the Kronecker delta symbol. For the Fourier harmonics of the tangential τ, φ -field components we get

$$\mathbf{E}_2^i \cdot \boldsymbol{\tau} = e_{m,\tau}^p(\eta) \cos(m+1)\varphi, \quad \mathbf{E}_2^i \cdot \mathbf{e}_\varphi = e_{m,\varphi}^p(\eta) \sin(m+1)\varphi,$$

$$\mathbf{H}_2^i \cdot \boldsymbol{\tau} = h_{m,\tau}^p(\eta) \sin(m+1)\varphi, \quad \mathbf{H}_2^i \cdot \mathbf{e}_\varphi = h_{m,\varphi}^p(\eta) \cos(m+1)\varphi,$$

where $\boldsymbol{\tau}$ is a tangential vector to the generatrix \mathfrak{Z} and \mathbf{e}_φ is a unit vector of the cylindrical coordinate system.

According to this for the P-polarized exciting plane wave (3) we use the following electric and magnetic vector potentials corresponding to the multipoles

$$\begin{aligned} \mathbf{A}_{mn}^{e,l}(\mathbf{r}) &= \{g_m^e(\eta, z_n) \cos(m+1)\varphi; -g_m^e(\eta, z_n) \sin(m+1)\varphi; \\ &\quad -f_{m+1}(\eta, z_n) \cos(m+1)\varphi\}, \\ \mathbf{A}_{mn}^{h,l}(\mathbf{r}) &= \{g_m^h(\eta, z_n) \sin(m+1)\varphi; g_m^h(\eta, z_n) \cos(m+1)\varphi; \\ &\quad -f_{m+1}(\eta, z_n) \sin(m+1)\varphi\}, \\ \mathbf{A}_{0n}^{e,h,l}(\mathbf{r}) &= \{0; 0; g_0^{h,e}(\eta, z_n)\}; \quad \zeta = 0, 1, 2; \end{aligned} \quad (4)$$

here $g_m^{e,h}, f_m$ are the Fourier harmonics related to the Green tensor components, which takes the form of Weyl-Sommerfeld integrals

$$\begin{aligned} g_m^{e,h}(\eta, z_n) &= \int_0^\infty J_m(\lambda \rho) v_{11}^{e,h}(z, z_n, \lambda) \lambda^{1+m} d\lambda, \\ f_m(\eta, z_n) &= \int_0^\infty J_m(\lambda \rho) v_{31}(z, z_n, \lambda) \lambda^{1+m} d\lambda. \end{aligned} \quad (5)$$

where (ρ, φ, z) are the cylindrical coordinates, point $\eta = (\rho, z)$ belongs to the semi-plane $\varphi = 0$. Here $\{z_n\}_{n=1}^\infty$ is a dense set of DS coordinates distributed over a segment $I_0^z \in D_i$ of the axis of symmetry and $v_{11}^{e,h}(z, z_n, \lambda), v_{31}(z, z_n, \lambda)$ are the corresponding spectral functions, which provide the continuity of the tangential field components at the interfaces $\Sigma_{0,1}$ and can be represented as follows

$$v_{11}^{e,h} = \begin{cases} \frac{\exp(-\eta_2 |z - z_n|)}{\eta_2} + A_2^{e,h+}(\lambda, z_n) \exp(-\eta_2 |z - d|), & z \geq d, z_n > d \\ A_1^{e,h-}(\lambda, z_n) \exp(-\eta_1 |z - d|) + A_1^{e,h+}(\lambda, z_n) \exp(-\eta_1 z), & d \geq z \geq 0; \\ A_0^{e,h-}(\lambda, z_n) \exp(\eta_0 z), & z \leq 0 \end{cases}$$

$$v_{31}^{e,h} = \begin{cases} B_2^{e,h+}(\lambda, z_n) \exp(-\eta_2 |z - d|), & z \geq d, z_n > d \\ B_1^{e,h-}(\lambda, z_n) \exp(-\eta_1 |z - d|) + B_1^{e,h+}(\lambda, z_n) \exp(-\eta_1 z), & d \geq z \geq 0; \\ B_0^{e,h-}(\lambda, z_n) \exp(\eta_0 z), & z \leq 0 \end{cases}$$

where $\eta_\zeta^2 = \lambda^2 - k_\zeta^2$. The spectral coefficients A and B can be determined from the one dimensional transmission conditions at $z=0, d$, which takes the following form [20]:

$$[v_{11}^e] = \left[\frac{1}{\mu} \frac{\partial v_{11}^e}{\partial z} \right] = 0, \quad [v_{11}^h] = \left[\frac{1}{\varepsilon} \frac{\partial v_{11}^h}{\partial z} \right] = 0,$$

$$\left[\frac{1}{\mu} v_{31}^e \right] = 0, \quad \left[\frac{1}{\varepsilon \mu} \frac{\partial v_{31}^e}{\partial z} \right] = - \left[\frac{1}{\varepsilon \mu} \right] v_{11}^e,$$

$$\left[\frac{1}{\varepsilon} v_{31}^h \right] = 0, \quad \left[\frac{1}{\varepsilon \mu} \frac{\partial v_{31}^h}{\partial z} \right] = - \left[\frac{1}{\varepsilon \mu} \right] v_{11}^h.$$

Where $[\]$ is a jump of values. In particular, the equality $v_{31}^e = v_{31}^h$ holds under $z \geq d$.

For the total field inside particle D_i we choose the following vector potentials [16]

$$\begin{aligned} \mathbf{A}_{mn}^{e,i}(\mathbf{r}) &= \{J_m^i(\eta, z_n) \cos(m+1)\varphi; -J_m^i(\eta, z_n) \sin(m+1)\varphi; 0\}, \\ \mathbf{A}_{mn}^{h,i}(\mathbf{r}) &= \{J_m^i(\eta, z_n) \sin(m+1)\varphi; J_m^i(\eta, z_n) \cos(m+1)\varphi; 0\}, \\ \mathbf{A}_n^{e,h,i}(\mathbf{r}) &= \{0; 0; J_0^i(\eta, z_n)\}; \end{aligned} \quad (6)$$

where $J_m^i(\eta, z_n) = j_m(k_i R_{\eta z_n})(\rho/R_{\eta z_n})^m$, and j_m are the spherical Bessel functions. Let us introduce the following notations:

$$\mathbf{D}_1^l = \begin{pmatrix} j/k\varepsilon_l \mu_l \nabla \times \nabla \times \\ -1/\mu_l \nabla \times \end{pmatrix}, \quad \mathbf{D}_2^l = \begin{pmatrix} 1/\varepsilon_l \nabla \times \\ j/k\varepsilon_l \mu_l \nabla \times \nabla \times \end{pmatrix}.$$

Now we can represent the approximate solution of the scattering problem for the P-polarized excitation [16]:

$$\begin{aligned} \begin{pmatrix} \mathbf{E}_N^l \\ \mathbf{H}_N^l \end{pmatrix} &= \sum_{m=0}^M \sum_{n=1}^{N_m^l} \left\{ p_{mn}^l \mathbf{D}_1^l \mathbf{A}_{mn}^{e,l} + q_{mn}^l \mathbf{D}_2^l \mathbf{A}_{mn}^{h,l} \right\} \\ &\quad + \sum_{n=1}^{N_0^l} r_n^l \mathbf{D}_1^l \mathbf{A}_n^{e,l}; \quad l = 2, i. \end{aligned} \quad (7)$$

The last term in (7) is associated with vertical electric dipoles. Here, N is a complex index incorporating M and N_m^l . We emphasize that in frame of the DSM, the scattered field $\{\mathbf{E}_N^l, \mathbf{H}_N^l\}$ in domains $D_{0,1,2}$ can be represented in terms of the unitary set of amplitudes $\{p_{mn}^2, q_{mn}^2, r_n^2\}$ due to the fact that the transmission

conditions at the interfaces $\Sigma_{0,1}$ are satisfied by incorporating the Green's tensor components (5) [16].

Let us next consider S-polarization of the exciting plane wave

$$\begin{aligned} \mathbf{E}_2^i(\mathbf{r}) &= T_2^S \mathbf{e}_y \exp\{-jk_2(x \sin \theta_2 + z \cos \theta_2)\}, \\ \mathbf{H}_2^i(\mathbf{r}) &= T_2^S n_2 (-\mathbf{e}_x \cos \theta_2 + \mathbf{e}_z \sin \theta_2) \exp\{-jk_2(x \sin \theta_2 + z \cos \theta_2)\}, \end{aligned} \quad (8)$$

where the T_2^S transmission coefficient associated with interfaces $\Sigma_{0,1}$

The Fourier components are taking the form

$$\begin{aligned} \mathbf{E}_2^i \cdot \boldsymbol{\tau} &= e_{m,\tau}^S(\eta) \sin(m+1)\varphi, & \mathbf{E}_2^i \cdot \mathbf{e}_\varphi &= e_{m,\varphi}^S(\eta) \cos(m+1)\varphi. \\ \mathbf{H}_2^i \cdot \boldsymbol{\tau} &= h_{m,\tau}^S(\eta) \cos(m+1)\varphi, & \mathbf{H}_2^i \cdot \mathbf{e}_\varphi &= h_{m,\varphi}^S(\eta) \sin(m+1)\varphi. \end{aligned}$$

To take into account the polarization of the external excitation in S-case (8) the following electric and magnetic potentials are used

$$\begin{aligned} \mathbf{A}_{mn}^{e,l}(\mathbf{r}) &= \{g_m^e(\eta, z_n) \sin(m+1)\varphi; g_m^e(\eta, z_n) \cos(m+1)\varphi; \\ &\quad -f_{m+1}(\eta, z_n) \sin(m+1)\varphi\}, \\ \mathbf{A}_{mn}^{h,l}(\mathbf{r}) &= \{g_m^h(\eta, z_n) \cos(m+1)\varphi; -g_m^h(\eta, z_n) \sin(m+1)\varphi; \\ &\quad -f_{m+1}(\eta, z_n) \cos(m+1)\varphi\} \\ \mathbf{A}_{0n}^{e,h,l}(\mathbf{r}) &= \{0; 0; g_0^{h,e}(\eta, z_n)\}. \end{aligned} \quad (9)$$

So, for S-polarization the approximate solution accepts the following form:

$$\begin{aligned} \begin{pmatrix} \mathbf{E}_N^l \\ \mathbf{H}_N^l \end{pmatrix} &= \sum_{m=0}^M \sum_{n=1}^{N_n^l} \left\{ p_{mn}^l \bar{\mathbf{D}}_1^l \mathbf{A}_{mn}^{e,l} + q_{mn}^l \bar{\mathbf{D}}_2^l \mathbf{A}_{mn}^{h,l} \right\} \\ &+ \sum_{n=1}^{N_0^l} r_n^l \bar{\mathbf{D}}_2^l \mathbf{A}_n^{h,l}, \quad l=2,i. \end{aligned} \quad (10)$$

The last term in (10) is associated with vertical magnetic dipoles [20]. The difference between (7) and (10) is caused by the fact that for S-polarization vector \mathbf{H}_2^i belongs to the incident plane.

The completeness of the system of lowest-order distributed multipoles used in (7) and (10) guarantees the convergence of the approximate solution to the exact one in any closed subset of D_2 [21].

3. Numerical scheme

As mentioned above the representations (7) and (10) satisfy all the conditions of the scattering problem (1) except the transmission conditions at the particle surface (2). These conditions are employed to determine the unknown amplitudes of the DS $\{p_{mn}^{2,i}, q_{mn}^{2,i}, r_n^{2,i}\}$. Because the scattering problem geometry is axially symmetric with respect to the Z-axis and the DS are distributed along the axis of symmetry, the problem of fulfilling the transmission conditions (2) at the surface ∂D_i can be reduced to the sequential solution of the transmission problems for the Fourier harmonics of the fields. Thus, instead of matching fields at the scattering surface, we can match their Fourier harmonics. Reducing the approximation problem on the surface leads to a set of problems enforced at the particle surface generatrix \mathfrak{V} . The unknown vector of DS amplitudes $\{p_{mn}^{2,i}, q_{mn}^{2,i}, r_n^{2,i}\}$ can be determined as a pseudo solution of an

over-determined system of linear equations

$$\mathbf{B}_m \mathbf{p}_m = \mathbf{q}_m, \quad m=0, \dots, M,$$

here \mathbf{B}_m is a rectangular matrix $\mathbf{B}_m = [B_{\kappa\kappa'}^m]$, $\kappa=1, \dots, 4L$, $\kappa'=1, \dots, 2(N_1^m + N_2^m)$. It was found that the reasonable ratio between number of matching points and the number of DS is $2 < L/(N_1^m + N_2^m) < 4$. In this case the vector of unknown amplitudes \mathbf{p}_m has the length of $2(N_1^m + N_2^m)$ and the vector in the right-hand side can be represented as $4L$ vector in the following form:

$$\mathbf{q}_m = (e_m^\tau(\eta_\kappa), e_m^\varphi(\eta_\kappa), h_m^\tau(\eta_\kappa), h_m^\varphi(\eta_\kappa))^T.$$

The components of the vector for the P-polarized excitation can be written as:

$$\begin{aligned} e_{m,\tau}^P(\eta) &= -(-j)^m T_2^P \{\alpha \cos \theta_2 [J_m(k_2 \rho \sin \theta_2) - J_{m+2}(k_2 \rho \sin \theta_2)] \\ &\quad + 2j\beta \sin \theta_2 J_{m+1}(k_2 \rho \sin \theta_2)\} \times \exp\{-jk_2 z \cos \theta_2\}, \\ e_{m,\varphi}^P(\eta) &= -\cos \theta_2 (-j)^m T_2^P [J_m(k_2 \rho \sin \theta_2) \\ &\quad + J_{m+2}(k_2 \rho \sin \theta_2)] \exp\{-jk_2 z \cos \theta_2\}, \\ h_{m,\tau}^P(\eta) &= -\alpha (-j)^m T_2^P n_2 [J_m(k_2 \rho \sin \theta_2) \\ &\quad + J_{m+2}(k_2 \rho \sin \theta_2)] \exp\{-jk_2 z \cos \theta_2\}, \\ h_{m,\varphi}^P(\eta) &= -(-j)^m T_2^P n_2 [J_m(k_2 \rho \sin \theta_2) \\ &\quad - J_{m+2}(k_2 \rho \sin \theta_2)] \exp\{-jk_2 z \cos \theta_2\}. \end{aligned}$$

where T_2^P is

$$T_2^P = \frac{t_{01}^P t_{12}^P \exp(-jk_1 \cos \theta_1 d)}{1 + r_{01}^P r_{12}^P \exp(-2jk_1 \cos \theta_1 d)},$$

Here θ_1 is the angle of refraction inside D_1 following to Snell's law, and

$$t_{iv}^P = \frac{2n_i \cos \theta_i}{n_i \cos \theta_v + n_v \cos \theta_i}, \quad r_{iv}^P = \frac{n_i \cos \theta_v - n_v \cos \theta_i}{n_i \cos \theta_v + n_v \cos \theta_i},$$

are the corresponding coefficients of transmission and reflection at the interface between the D_i and D_v domains.

In case of S-polarized excitation the components accept the following form:

$$\begin{aligned} e_{m,\tau}^S(\eta) &= \alpha (-j)^m T_2^S [J_m(k_2 \rho \sin \theta_2) + J_{m+2}(k_2 \rho \sin \theta_2)] \exp\{-jk_2 z \cos \theta_2\}, \\ e_{m,\varphi}^S(\eta) &= (-j)^m T_2^S [J_m(k_2 \rho \sin \theta_2) - J_{m+2}(k_2 \rho \sin \theta_2)] \exp\{-jk_2 z \cos \theta_2\}, \\ h_{m,\tau}^S(\eta) &= -(-j)^m T_2^S n_2 \{\alpha \cos \theta_2 [J_m(k_2 \rho \sin \theta_2) - J_{m+2}(k_2 \rho \sin \theta_2)] \\ &\quad - 2j\beta \sin \theta_2 J_{m+1}(k_2 \rho \sin \theta_2)\} \times \exp\{-jk_2 z \cos \theta_2\}, \\ h_{m,\varphi}^S(\eta) &= -\cos \theta_2 (-j)^m T_2^S n_2 [J_m(k_2 \rho \sin \theta_2) \\ &\quad + J_{m+2}(k_2 \rho \sin \theta_2)] \exp\{-jk_2 z \cos \theta_2\} \end{aligned}$$

$$T_2^S = \frac{t_{01}^S t_{12}^S \exp(-jk_1 \cos \theta_1 d)}{1 + r_{01}^S r_{12}^S \exp(-2jk_1 \cos \theta_1 d)},$$

and

$$t_{iv}^S = \frac{2n_i \cos \theta_i}{n_i \cos \theta_i + n_v \cos \theta_v}, \quad r_{iv}^S = \frac{n_i \cos \theta_i - n_v \cos \theta_v}{n_i \cos \theta_i + n_v \cos \theta_v},$$

here $(\alpha, 0, \beta)$ is a vector, tangential to the particle meridian at η -point and (ρ, z) are cylindrical coordinates of the matching points. Because the Fourier harmonics do not depend on the φ -angle, the linear system corresponding to vertical electric or magnetic dipoles for both polarizations can be written as

$$\mathbf{B}_{-1} \mathbf{p}_{-1} = \mathbf{q}_{-1},$$

where matrix \mathbf{B}_{-1} has twice smaller dimension $2L \times (N_1^m + N_2^m)$, the right-hand side vector has the length of $2L$ and the vector of amplitudes has the length of $(N_1^m + N_2^m)$.

Then for P -polarization we have

$$e_{-1,\tau}^P(\eta) = T_2^P [j\alpha \cos \theta_2 J_1(k_2 \rho \sin \theta_2) + \beta \sin \theta_2 J_0(k_2 \rho \sin \theta_2)] \exp\{-jk_2 z \cos \theta_2\}$$

$$h_{-1,\varphi}^P(\eta) = jT_2^P n_2 J_1(k_2 \rho \sin \theta_2) \exp\{-jk_2 z \cos \theta_2\}.$$

And for S -polarization:

$$e_{-1,\varphi}^S(\eta) = -jT_2^S J_1(k_2 \rho \sin \theta_2) \exp\{-jk_2 z \cos \theta_2\},$$

$$h_{-1,\tau}^S(\eta) = -T_2^S n_2 [j\alpha \cos \theta_2 J_1(k_2 \rho \sin \theta_2) + \beta \sin \theta_2 J_0(k_2 \rho \sin \theta_2)] \exp\{-jk_2 z \cos \theta_2\}.$$

As the DSM is a direct method it allows solving the scattering problem for the entire set of the incident angles θ_0 and both polarizations (P and S) at once. Besides, the numerical scheme provides an opportunity to control the convergence of the approximate solution by the posterior error estimation [20].

After the amplitudes of the DS have been determined, one can compute the far field pattern $\mathbf{F}(\theta, \varphi)$ of the scattered field, which is determined in the upper $\Omega = \{0^\circ \leq \theta < 90^\circ, 0^\circ \leq \varphi \leq 360^\circ\}$ or lower $\Omega = \{90^\circ \leq \theta < 180^\circ, 0^\circ \leq \varphi \leq 360^\circ\}$ parts of the unite semi-sphere and is given by

$$\mathbf{E}_2^s(\mathbf{r}) / |\mathbf{E}^0(z=0)| = \frac{\exp\{-jk_0 r\}}{r} \mathbf{F}(\theta, \varphi) + O(r^{-2}) \quad z > 0, r \rightarrow \infty,$$

Here

$$\mathbf{F}(\theta, \varphi) = F_{\theta}^{P,S} \mathbf{e}_\theta + F_{\varphi}^{P,S} \mathbf{e}_\varphi.$$

By asymptotical estimation of the Weyl–Sommerfeld integrals involved in (5) the representation of the elements of the far field pattern takes the form of a finite linear combination of elementary functions [20]

$$F_{0,2(\theta)}^P(\theta, \varphi) = jk \sum_{m=0}^M (jk_{0,2} \sin \theta)^m \cos(m+1)\varphi \sum_{n=1}^{N_m^2} \left\{ p_{nm}^{2,P} [\bar{g}_{nm}^{e(0,2)} \cos \theta + jk_{0,2} \sin^2 \theta \bar{f}_{nm}^{e(0,2)}] + \sqrt{\frac{\mu_{0,2}}{\varepsilon_{0,2}}} q_{nm}^{2,P} \bar{g}_{nm}^{h(0,2)} \right\} - jk \sin \theta \sum_{n=1}^{N_m^2} r_n^{2,P} \bar{g}_{n0}^{h(0,2)},$$

$$F_{0,2(\varphi)}^P(\theta, \varphi) = -jk \sum_{m=0}^M (jk_{0,2} \sin \theta)^m \sin(m+1)\varphi \times \sum_{n=1}^{N_m^2} \left\{ p_{nm}^{2,P} \bar{g}_{nm}^{e(0,2)} + \sqrt{\frac{\mu_{0,2}}{\varepsilon_{0,2}}} q_{nm}^{2,P} [\bar{g}_{nm}^{h(0,2)} \cos \theta + jk_{0,2} \sin^2 \theta \bar{f}_{nm}^{h(0,2)}] \right\}. \quad (11)$$

For S -polarized external excitation the components of the far field pattern components accept the form

$$F_{0,2(\theta)}^S(\theta, \varphi) = jk \sum_{m=0}^M (jk_{0,2} \sin \theta)^m \sin(m+1)\varphi \sum_{n=1}^{N_m^2} \left\{ p_{nm}^{2,S} [\bar{g}_{nm}^{e(0,2)} \cos \theta + jk_{0,2} \sin^2 \theta \bar{f}_{nm}^{e(0,2)}] - \sqrt{\frac{\mu_{0,2}}{\varepsilon_{0,2}}} q_{nm}^{2,S} \bar{g}_{nm}^{h(0,2)} \right\}.$$

$$F_{0,2(\varphi)}^S(\theta, \varphi) = jk \sum_{m=0}^M (jk_{0,2} \sin \theta)^m \cos(m+1)\varphi \sum_{n=1}^{N_m^2} \left\{ p_{nm}^{2,S} \bar{g}_{nm}^{e(0,2)} + \sqrt{\frac{\mu_{0,2}}{\varepsilon_{0,2}}} q_{nm}^{2,S} [\bar{g}_{nm}^{h(0,2)} \cos \theta + jk_{0,2} \sin^2 \theta \bar{f}_{nm}^{h(0,2)}] \right\}.$$

$$- \sqrt{\frac{\mu_{0,2}}{\varepsilon_{0,2}}} q_{nm}^{2,S} \left[\bar{g}_{nm}^{h(0,2)} \cos \theta + jk_{0,2} \sin^2 \theta \bar{f}_{nm}^{h(0,2)} \right] \left. \right\} + jk \sqrt{\frac{\mu_{0,2}}{\varepsilon_{0,2}}} \sin \theta \sum_{n=1}^{N_m^2} r_n^{2,S} \bar{g}_{nm}^{e(0,2)}, \quad (12)$$

here $\{p_{nm}^{2,(P,S)}, q_{nm}^{2,(P,S)}, r_n^{2,(P,S)}\}$ are the Fourier harmonics of the DS amplitudes corresponding to P/S polarizations and the associating spectral functions $\bar{g}_{nm}^{e,h} \bar{f}_{nm}$ can be written as

$$\bar{g}_{nm}^{e,h(2)}(\theta) = \exp[jk_2 z_n \cos \theta] + jk_2 \cos \theta \exp[jk_2 d \cos \theta] A_2^{e,h+}(k_2 \sin \theta, z_n),$$

$$\bar{f}_{nm}^{e,h(2)}(\theta) = jk_2 \cos \theta \exp[jk_2 d \cos \theta] B_2^{e,h+}(k_2 \sin \theta, z_n).$$

$$\bar{g}_{nm}^{h(0)}(\theta) = jk_0 \cos \theta A_0^{e,h-}(k_0 \sin \theta, z_n),$$

$$\bar{f}_{nm}^{h(0)}(\theta) = jk_0 \cos \theta B_0^{e,h-}(k_0 \sin \theta, z_n).$$

Hence, after the unknown amplitudes of the DS are determined, the far field patterns for P and S -polarized excitation are represented as the finite linear combinations of elementary functions. This circumstance ensures fast and effective computer analysis of scattering characteristics in the far zone.

4. Results and discussion

In this section we present some computer simulation results for the conversion of evanescent waves into the scattered ones by a particle deposited above a metal-filmed glass prism. We consider the Differential Scattering Cross-Section (DSC), which is given by

$$DSC_{0,2}^{P,S}(\theta_0, \theta, \varphi) = \left| F_{0,2(\theta)}^{P,S}(\theta_0, \theta, \varphi) \right|^2 + \left| F_{0,2(\varphi)}^{P,S}(\theta_0, \theta, \varphi) \right|^2 \quad (13)$$

Here the components of the far field pattern are given by (11)–(12). The dimension of $DSC_{0,1}^{P,S}$ is μm^2 units. In this part we also examine the objective response as a function of height of the particle above the surface. It represents the integrated intensity scattered into the prescribed solid angle Ω

$$\sigma_{0,2}^{P,S}(\theta_0) = \int_{\Omega} DSC_{0,2}^{P,S}(\theta_0, \theta, \varphi) d\omega, \quad (14)$$

where Ω corresponds to the numerical aperture of the objective lens. The integral response is used to evaluate the scattered intensity captured by the objective lens [15].

Let us consider a P or S -polarized plane wave with a wavelength of $\lambda=658$ nm. The prism is made of N-LASF46A glass with a refractive index for this wavelength of $n_0=1.8951$. We consider polystyrene latex (PSL) particles with a refractive index $n_i=1.59$ and diameters of $D=300$ nm, 600 nm and 1.2 μm , which are deposited in water with $n_2=1.3306$ on a gold film with $n_1=0.1425-3.6821j$ of thickness $d=51$ nm. The refractive indices were taken from [22]. The deposition of the gold film on the prism surface enables to increase the penetration depth (up to 720 nm) and a light reflectivity [6]. The critical angle for this system at which the evanescent waves appear is 44.6° . Scattered fields are captured by objectives with a collecting angle of 30° . For technical reasons, the collector situated beneath the prism has a central cut of 5° to avoid the specular beam.

In this particular case it is easy to estimate that PR related to the minimum value of the reflection coefficient for P-polarized excitation has the form

$$R_{02}^p(\theta_0) = \frac{r_{01}^p + r_{12}^p \exp\{-2jk_1 \cos\theta_1 d\}}{1 + r_{01}^p r_{12}^p \exp\{-2jk_1 \cos\theta_1 d\}}, \quad (15)$$

which corresponds to the incident angle $\theta_0 = 48.96^\circ$. Here r_{01}, r_{12} are the reflection coefficients from the boundaries Σ_0, Σ_1 and θ_1 is the angle of refraction into the film. The behavior of the reflection coefficient (15) can be observed in Fig. 3.

In the following figures the results of computer simulation analysis are presented. The incident angle $\theta_0 = 48.96^\circ$ has been chosen to reduce the plane wave reflection in the specular direction. In Fig. 4 the objective response $\sigma_{0,2}^{p,s}$ versus particle–film distance h is presented for PSL particle of $D=300$ nm for both polarization of the incident light and for two positions of the collector: above (conventional TIRM scheme) and beneath the prism. From the behavior of the curves one can see that the intensity of P-polarized light is several orders higher than for the S-polarized one. Another observation is that both curves

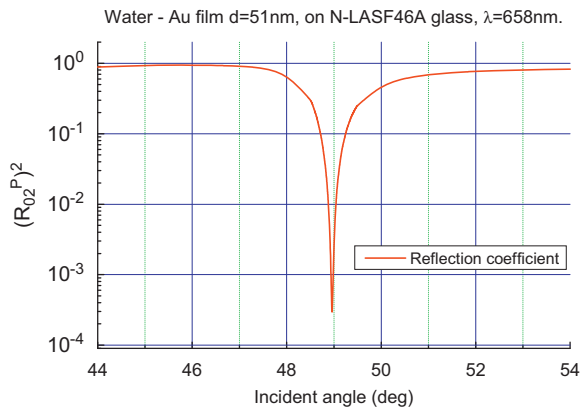


Fig. 3. Reflection coefficient (15) from prism–film interface for P-polarized plane wave in water versus the incident angle θ_0 .

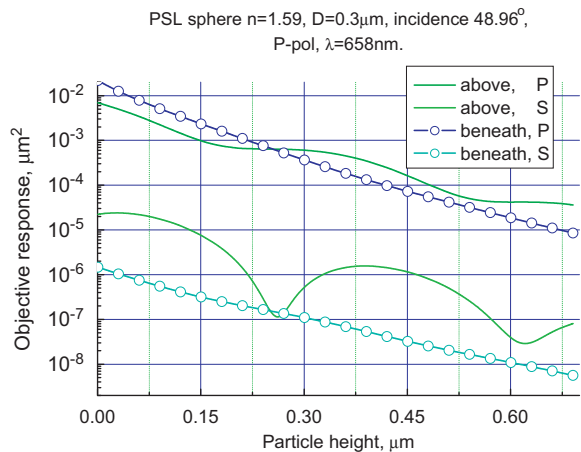


Fig. 4. Integrated intensity (14) versus particle height for PSL particle of $D=0.3$ μm for two collectors depositions and P and S polarizations of the incident light.

for the collector deposition above the prism demonstrate pronounced oscillations. At some points of those curves the value of σ_0^p seems to be the same at different heights. The last circumstance faces the problem of precise determination of particle–film distance from the measured data without additional information. Similar oscillations have been detected in [23]. At the same time both curves for the collector deposited beneath the prism have strongly monotonic decrease and allow the single-valued determination of the particle position above the film from the measured response. To verify our observation in Figs. 5 and 6 similar results are shown for particles of $D=600$ nm and $D=1.2$ μm respectively. The results are in good agreement with those for smaller particle, presented above. For the collector deposited in the upper half-space both P and S-polarized curves demonstrate oscillations or flat plateaus, while both curves for the collector beneath the prism are monotonic.

Now we try to explain these results by analyzing the behavior of the DSC in the incidence plane. For these investigations we take the particle of $D=600$ nm and two particle–film distances where σ_0^p reaches close values. The

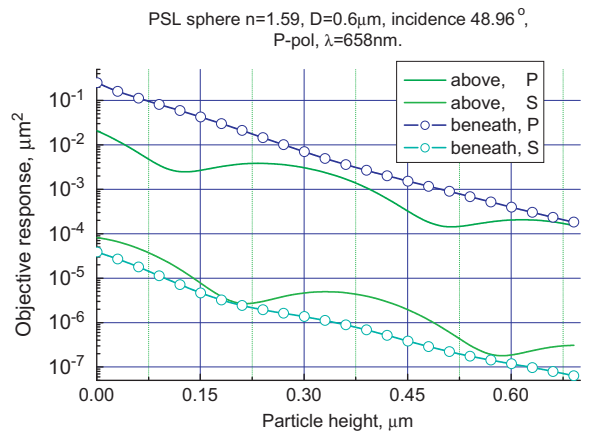


Fig. 5. Integrated intensity for PSL particle of $D=0.6$ μm for two collectors depositions and P and S polarizations of the incident light.

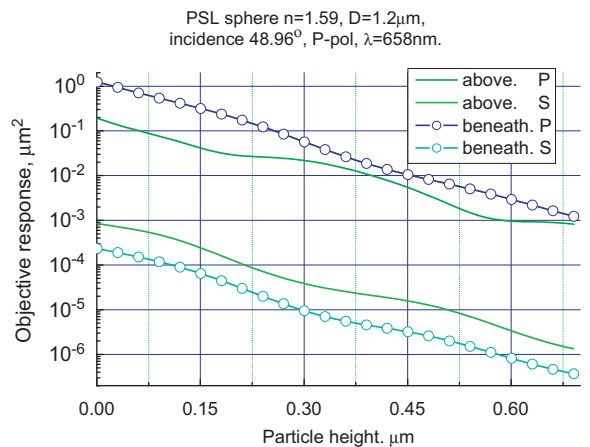


Fig. 6. Integrated intensity for PSL particle of $D=1.2$ μm for two collectors depositions and P and S polarizations of the incident light.

results for the DSC distribution are presented in Fig. 7. Here the range of observation angles $90^\circ < \theta < 270^\circ$ belongs to the lower semi-plane (glass) and the ranges of $0^\circ < \theta < 90^\circ$ and $270^\circ < \theta < 360^\circ$ belong to the upper semi-plane (water).

From the figures one can see that the maximum of intensity in the prism domain is directed towards the specular direction at $\theta \approx 135^\circ$ and the maximum in the upper semi-plane is directed far from the upper collector. In Figs. 7 and 8 the heights were chosen so, that the values of the responses for both heights of the upper collector were almost identical. From the results presented above one can see that, regardless the fact that in the

upper semi-plane the intensity values of both curves are nearly the same (at the range from -30° to $+30^\circ$), in the lower semi-plane, both values near the specular direction clearly differ. Due to this circumstance the determination of the particle–film distance from observations of the intensity beneath the prism should be much easier in contrast to the conventional observations in the upper domain. The same situation occurs for the particles of the other refractive index (melanine as an example).

5. Conclusion

In this paper we have analyzed the scattering of the polarized light by a particle deposited above the filmed surface for TIRM applications. The simulation results based on the DSM computer model have been presented and discussed. The results have demonstrated that the intensity of P-polarized light exceeds the S-polarized one by several orders. In connection with this we would like to point out that E_z does not exist in S-polarized field. Besides, computer simulation showed that the response in the prism domain mostly exceeds the response in the water domain. Additionally, the behavior of the collector response beneath the prism demonstrates monotonic exponential decay versus particle height that enables easier determination of the particle–film distance, while the response measured above the film does not allow a single-valued determination of the particle–film distance. From this analysis, we conclude that the alternative TIRM scheme with collector deposited beneath the prism gives considerable advantages compared to the conventional one. This circumstance should be taken into account while setting up new TIRM designs.

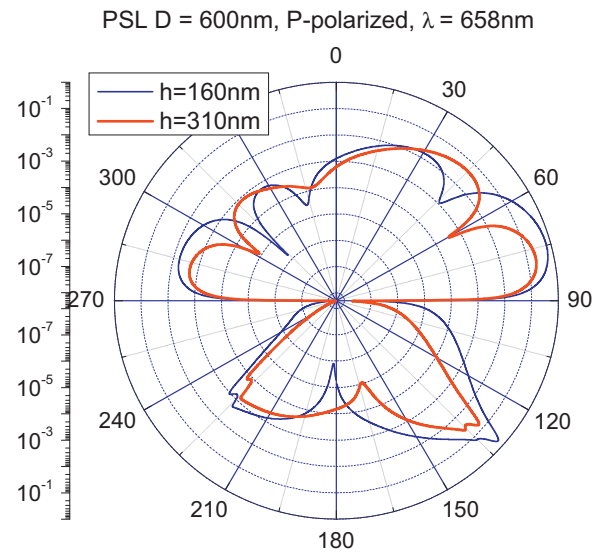


Fig. 7. Scattered intensity in the incidence plane for the particle of $D=0.6 \mu\text{m}$ for different particle–film distances h , P-polarization.

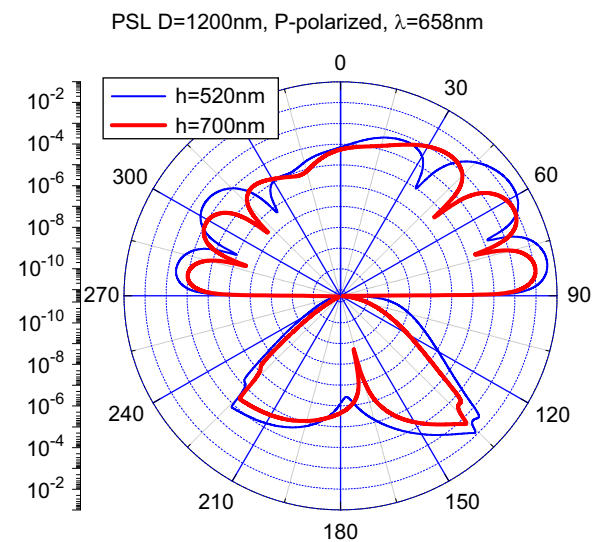


Fig. 8. Scattered intensity in the incidence plane for the particle of $D=1.2 \mu\text{m}$ for different particle–film distances h , P-polarization.

Acknowledgement

We gratefully acknowledge funding of this research by Deutsche Forschungsgemeinschaft (DFG) and the Russian Foundation for Basic Research (RFBR).

References

- [1] Walz J. Measuring particle interactions with total internal reflection microscopy. *Curr Opin Colloid Interfac Sci* 1997;2:600–6.
- [2] Prieve DC. Measurement of colloidal forces with TIRM. *Adv Colloid Interfac Sci* 1999;82:93–125.
- [3] Ducker W, Senden T, Pashley R. Direct measurement of colloidal forces using an atomic force microscope. *Nature* 1991;353:239–41.
- [4] Berg-Sorensen K, Flyvbjerg H. Power spectrum analysis for optical tweezers. *Rev Sci Instrum* 2004;75:594–612.
- [5] Volpe G, Volpe G, Petrov D. Brownian motion in a nonhomogeneous force field and photonic force microscope. *Phys Rev E* 2007;76(6): 118–27.
- [6] Volpe G, Brettschneider T, Helden L, Bechinger C. Novel perspectives for the application of total internal reflection microscopy. *Opt Exp* 2009;17(26):23975–23985.
- [7] Ommering K, Somers PA, Koets M, Schleipen JJHB, Jzendoorn LJ, Prins MWJ. Mobility and height detection of particle labels in an optical evanescent wave biosensor with single-label resolution. *J Phys D: Appl Phys* 2010;43:155501.
- [8] Bijamov A, Shubitidze F, Oliver PM, Vezenov DV. Optical Response of Magnetic Fluorescent Microspheres Used for Force Spectroscopy in the Evanescent Field. *Langmuir* 2010;26(14):12003–11.
- [9] Bevan MA, Prieve DC. Direct Measurement of retarded van der Waals Attraction. *Langmuir* 1999;15:7925–36.

- [10] Hertlein C, Helden L, Gambassi A, Dietrich S, Bechinger C. Direct measurement of critical Casimir forces. *Nature* 2008;451:172–5.
- [11] Blickle V, Babić D, Bechinger C. Evanescent light scattering with magnetic colloids. *Appl Phys Lett* 2005;87:101–2.
- [12] Piech M, Weroniński P, Wu X, Walz JY. Prediction and measurement of the interparticle depletion interaction next to a flat wall. *J Colloid Interfac Sci* 2002;247:327–41.
- [13] Helden L, Roth R, Koenderink GH, Leiderer P, Bechinger C. Direct Measurement of Entropic Forces Induced by Rigid Rods. *Phys Rev Lett* 2003;90:048301.
- [14] Von Grunberg HH, Helden L, Leiderer P, Bechinger C. Measurement of surface charge densities on Brownian particles using total internal reflection microscopy. *J Chem Phys* 2001;114:10094–104.
- [15] Hertlein C, Riefler N, Eremina E, Wriedt T, Eremin Y, Helden L, Bechinger C. Experimental Verification of an Exact Evanescent Light Scattering Model for TIRM. *Langmuir (Letter)* 2008;24(1):1–4.
- [16] Eremin YuA, Sveshnikov AG. Mathematical models in nanooptics and biophotonics problems on the base of Discrete Sources Method. *Comput Maths Math Phys* 2007;47(2):262–79.
- [17] Helden L, Eremina E, Eremin Y, Riefler N, Hertlein C, Bechinger C, Wriedt T. Single particle evanescent light scattering simulations for total internal reflection microscopy. *Appl Optics* 2006;45:7299–308.
- [18] Riefler N, Eremina E, Hertlein C, Helden L, Eremin Y, Wriedt T, Bechinger C. Comparison of T-matrix method with discrete sources method applied for total internal reflection microscopy. *J Quantum Spectr Radiat Transfer* 2007;106:464–74.
- [19] Raether H. Surface Plasmon on Smooth and Rough Surfaces and on Gratings. Berlin: Springer; 1998 ch. 2.
- [20] Eremin YuA, Orlov NV, Sveshnikov AG. Models of Electromagnetic Scattering Problems Based on Discrete Sources Methods. In: Wriedt T, editor. *Generalized Multipole Techniques for Electromagnetic and Light Scattering*. Amsterdam: Elsevier Science; 1999. p. 39–79.
- [21] Doicu A, Yu Eremin, Wriedt T. Acoustic and electromagnetic scattering analysis using discrete sources. London: Academic Press; 2000.
- [22] <http://refractiveindex.info/>.
- [23] Eremina E, Grishina N, Eremin Y, Helden L, Wriedt T. Total Internal Reflection Microscopy with multilayered interface: light scattering model based on discrete sources method. *J Opt A: Pure Appl Opt* 2006;8:999–1006.